

Compatibility of Reduced Activation Ferritic/Martensitic Steels with Liquid Breeders

T. Muroga 1), T. Nagasaka 1), M. Kondo 1), A. Sagara 1), N. Noda 1), A. Suzuki 2),
T. Terai 2)

- 1) National Institute for Fusion Science, Oroshi, Toki, Gifu 509-5292, Japan
- 2) Graduate School of Engineering, The University of Tokyo, 7-3-1 Hongo, Bunkyo-ku,
Tokyo 113-8656, Japan

e-mail : muroga@nifs.ac.jp

Abstract. The compatibility of Reduced Activation Ferritic/Martensitic Steel (RAFM) with liquid Li and molten-salt Flibe have been characterized and assessed. Static compatibility tests were carried out in which the specimens were immersed into liquid Li or Flibe in isothermal autoclaves. Also carried out were compatibility tests in flowing liquid Li by thermal convection loops. In the case of liquid Li, the corrosion rate increased with temperature significantly. The corrosion was almost one order larger for the loop tests than for the static tests. Chemical analysis showed that the corrosion was enhanced when the level of N in Li is increased. Transformation from martensitic to ferritic phase and the resulting softening were observed in near-surface area of Li-exposed specimens, which were shown to be induced by decarburization. In the case of Flibe, the corrosion loss was much larger in a Ni crucible than in a RAFM crucible. Both fluorides and oxides were observed on the surfaces. Thus, the key corrosion process of Flibe is the competing process of fluoridation and oxidation. Possible mechanism of the enhanced corrosion in Ni crucible is electrochemical circuit effect. It was suggested that the corrosion loss rate of RAFM by liquid Li and Flibe can be reduced by reducing the level of impurity N in Li and avoiding the use of dissimilar materials in Flibe, respectively.

1. Introduction

Liquid Li, molten salt Flibe and Li-Pb are candidate tritium breeding materials for advanced liquid breeder blanket of fusion reactors. The Fe-Cr-W based Reduced Activation Ferritic/Martensitic Steels (RAFM) are regarded as the leading candidate for near and middle-term blankets of fusion reactors. Design efforts are being made for the breeding blankets using Li/RAFM [1], Flibe/RAFM [2] and Li-Pb/RAFM [3]. Although each liquid breeder system has pros and cons, compatibility with the structural materials is the common key issue. In contrast to some data available on the compatibility of RAFM with Li-Pb based on the recent efforts in European countries, the data with liquid Li and Flibe are quite limited.

The primary candidate structural materials for Li blanket have been vanadium-base alloys. Use of RAFM instead of vanadium-base alloys can reduce the necessary effort for materials development, although the blanket maximum operation temperature needs to be decreased from ~973K to 823K because of the limited high temperature strength of RAFM. Thus Li/RAFM system is regarded as a near-term candidate or a temporary candidate system toward a longer-term development of Li/vanadium-base alloy blanket. The Li/RAFM blanket has advantages of high heat removal capability and low tritium leakage. As to the corrosion of ferritic steels in Li, only studies on conventional Fe-Cr-Mo alloys are available [4]. In those studies, however, investigation on microstructure and micro-chemical processes was quite limited. Any study was not carried out for RAFM (Fe-Cr-W) steels yet.

Flibe blankets have advantages of low reactivity, easier tritium recovery and no MHD pressure drop. A blanket using combination of Flibe and RAFM has an issue of small temperature window (~723K to ~823K) because of high melting temperature of Flibe and limited high temperature strength of RAFM. Thus this system is regarded as a near-term candidate or a temporary candidate system toward a longer-term development of Flibe/vanadium-base alloy or Flibe/ODS-steel blanket. For corrosion of RAFM in Flibe, a study on the influence of REDOX control on dissolution rate of the constituent elements of RAFM was carried out in Japan-USA Cooperation Program JUPITER-II [5]. In that study, however, investigation on microstructure and micro-chemical processes was limited.

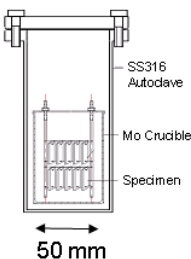
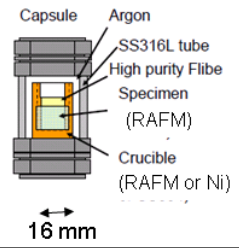
	Liquid Li	Flibe
Static Pot Tests	<p>100 ml</p> 	<p>2 ml</p> 
Natural Convection Loop $\Delta T = 50 \sim 100$ [K] $V = 0.01 \sim 0.05$ [m/s]	<p>700 ml</p> 	<p>200 ml</p> 

FIG. 1. Apparatus used in the present study.

The upper limit of the operation temperature of RAFM has been defined as ~ 823 K based on their high temperature strength. However, in this evaluation, compatibility with breeding materials was not taken into account, which could further limit the operation conditions. Evaluation of advantages of liquid Li, Flibe and Li-Pb systems is also necessary from the compatibility viewpoints.

Characterizations of the corrosion process have been carried out in National Institute for Fusion Science (NIFS) or by NIFS-University collaborations for RAFM/Li [6] and RAFM/Flibe [7] combinations. The purpose of this paper is to characterize and access the compatibility of RAFM with Li and Flibe in comparison with the reported Li-Pb data [8] for investigating feasibility of the RAFM/liquid breeder blankets.

2. Experimental

Specimens used in this study are Fe-9Cr-2W based RAFM steel (JLF-1:JOYO-2-HEAT) normalized at 1323K for 1 hr and tempered at 1053K for 1 hr. Static compatibility tests were carried out in which the specimens were immersed into liquid Li or Flibe in isothermal autoclaves. Also carried out were compatibility tests in flowing liquid Li and Flibe using natural convection loops. The apparatus of the present study is schematically shown in Fig. 1. The size of JLF-1 specimens used was 26x5x0.25 mm and 15x10x1 mm for Li and Flibe tests, respectively.

Static exposure experiments to liquid Li were carried out in a Mo cup with Mo specimen

TABLE 1. Summary of the experimental conditions

Melt	Test Method	Temperature (K)	Exposure Time (h)
Li	Static (Mo cup)	773	250
			750
		873	100
	Loop (316SS)	773/673*	250
			750
			750
			100
Loop (410SS)	753/633*	100	
Flibe	Static (JLF-1 crucible)	823	2000
	Static (Ni crucible)	823	2000

*hot-leg/cold-leg, nominal temperatures measured at loop exterior

holders, which were placed in a stainless steel autoclave. The detail of the static test facility was introduced in the previous paper [6]. In the case of Flibe, crucibles made from the JLF-1 and pure Ni were prepared. The size of the crucibles was 20 mm in outer diameter, 30 mm in height and 2 mm in wall thickness. A coupon specimen and 3-4 g of the Flibe was set into each crucible and were sealed in a stainless steel (SS304) capsule filled with high purity helium. High purity commercial Li (99.9%wt with the nominal N impurity level of 40ppm) and the Flibe (Fe, Cr, Ni < 10ppm) purified by HF gas and H₂ gas injection at 873 K were used for the exposure tests.

Exposure tests in flowing Li were carried out by two thermal convection loops, which were made of SS316L and SS410 stainless steels, and the both loops consisted of a loop pipe, a Li tank and a heating system. The detail of the SS316 loop was reported elsewhere [9]. The estimated flowing velocity in the loops was ~0.05 m/s. During the corrosion tests, the operating temperatures for the loop system were divided as: hot-leg region (753~773 K) and cold-leg region (~673 K). Specimens were fixed by Mo wires at each position. The impurity level in Li in the loop tests was expected to be comparable with the static experiments because of the similar preparing procedure. After exposure, liquid Li was drained away from the loop. Exposure in flowing Flibe was also carried out using a thermal convection loop with SS316. The examination of the specimens is remaining to be carried out, and thus the results are not reported in this paper. The experimental conditions are summarized in Table 1.

After the exposure to Li, the specimens were cleaned with water. After exposure to Flibe, the remaining Flibe on the specimen surface was dissolved and removed by a LiCl-KCl mixture.

The examinations of the specimens after the exposures were carried out for weight loss measurements by Electro-Balance with the accuracy of 0.1mg, surface morphology and composition by Scanning Electron Microscope (SEM) equipped with Energy Dispersive X-ray Spectrometer (EDS) and X-ray Photoelectron Spectroscopy (XPS), microstructure by Transmission Electron Microscope (TEM), and hardness by Vickers Hardness Test Machine.

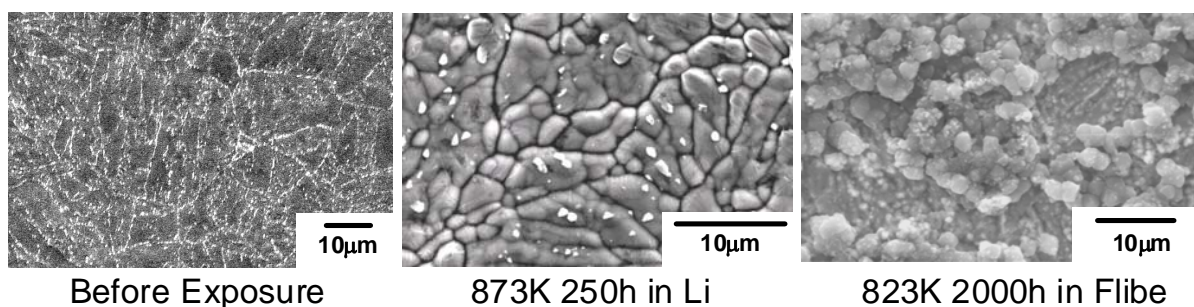


FIG. 2. Surface microstructure of JLF-1 before and after the exposure in static Li and Flibe.

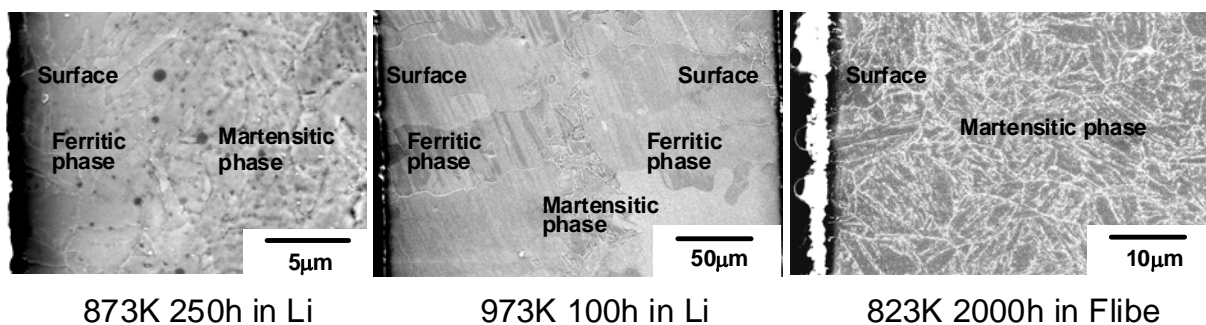


FIG. 3. Cross sectional microstructure of JLF-1 before and after the exposure in static Li and Flibe.

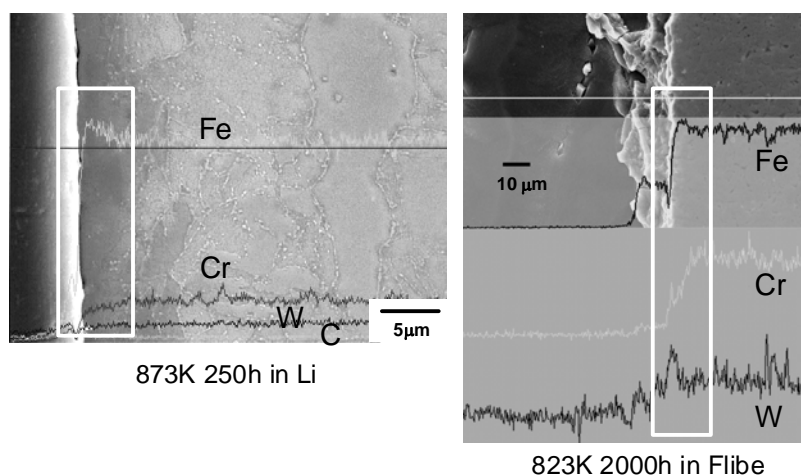


FIG. 4. EDS compositional depth profiles of JLF-1 after exposure in static Li and Flibe. The areas near the surfaces are emphasized by the squares.

3. Results

3.1 Microstructure

Fig.2 shows surface microstructural images of JLF-1 before exposure, after exposure in Li at 873K for 250h and in Flibe at 823K for 2000h. Before exposure, martensitic lath structure, grain boundaries and precipitates were observed. After exposure in Li, lath structure and precipitates disappeared. After exposure in Flibe, the surface was covered with corrosion products. Low angle XRD showed that they are fluorides (FeF_2 , CrF_2) and oxides (Li-Fe-O system or BeO). The remarkable change in Li-exposed specimens shows that the martensitic phase changed into ferritic phase.

Fig.3 is the cross sectional images of JLF-1 after exposure to Li at 873K for 250h and at 973K for 100h, and to Flibe at 823K for 2000h. The thickness of the ferritic phase was approximately 5 μm after exposure to Li at 873K and $\sim 100\mu\text{m}$ at 973K, indicating strong temperature dependence. No phase change was observed by exposure to Flibe at 823K.

3.2 Composition and hardness change

Fig. 4 compares the depth distribution of Fe, Cr and W levels in JLF-1 measured by SEM-EDS line scanning for the cases of exposure to Li and Flibe. Depletion of Cr near the surface was commonly observed for the both cases. However, W near the surface behaved differently, e.g. depleted in Li and enriched in Flibe.

The chemical analyses of the specimens after exposure to Li are listed in Table 2. Significant depletion of carbon at 973 K implies that the drastic phase change observed at 973 K is due to the loss of carbon from the martensitic phase. Change of other elements was small. In some cases, Li was sampled after the tests for chemical analysis. The results showed that the N level in Li after the test at 873K for 250h and 972K for 100h is 60 and 630 wppm, respectively.

TABLE 2. Chemical analysis of the specimens after exposure to Li in static tests. (wt%)

	C	Cr	W	N
Before exposure	0.09	8.92	2.00	0.01
773K 250h	0.09	8.80	1.95	0.01
873K 250h	0.09	8.83	1.93	0.02
973K 100h	0.03	8.88	1.95	0.01

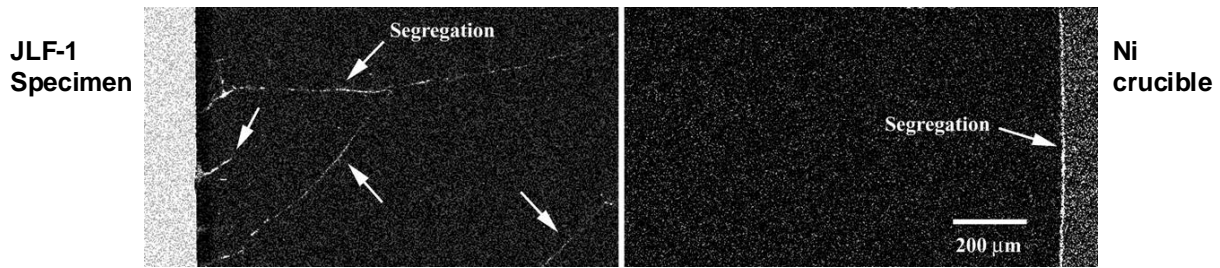


FIG. 5. EDS mapping of Fe in solidified Flibe near the JLF-1 specimen and the Ni crucible after an exposure at 823K and 2000h.

Fig. 5 is an EDS mapping of Fe in the solidified Flibe near the JLF-1 specimen and the Ni crucible after an exposure at 823K and 2000h. Segregation of dissolved Fe at line defects in Flibe and the surface of Ni crucible was detected, indicating that Fe transferred from the specimen to the crucible.

Fig. 6 shows cross sectional distribution of Vickers Hardness after exposure to Li and Flibe. In the case of Li, softening near the surface was enhanced with the increase of the test temperature. The depth of the softening at 973K (100-120μm) is close to the depth of the phase transformation shown in Fig. 3. More softening took place by the loop tests than the static tests. Only coarse data are available for Flibe showing no significant softening near the surface. The systematic difference in the bulk hardness between Li-exposed and Flibe-exposed specimens seems to be due to the difference in the applied load (10g for Li and 50g for Flibe) for the evaluation.

3.3 Corrosion loss

Fig. 7 summarizes the corrosion loss measured in the present experiments as a function of the exposure time. Fig. 7 shows that the corrosion by Li increased with the temperature and more corrosion occurred in the flowing loop test than the static test at the identical temperature. Also shown in Fig. 7 is much higher corrosion rate by Flibe in Ni crucible than in JLF-1 crucible. Fig. 7 includes the corrosion rate contour lines.

4. Discussion

Past experiments proved that the non-metal impurities, especially N, have a strong impact on the corrosion behavior of Li by forming binary or ternary compounds [10]. This could

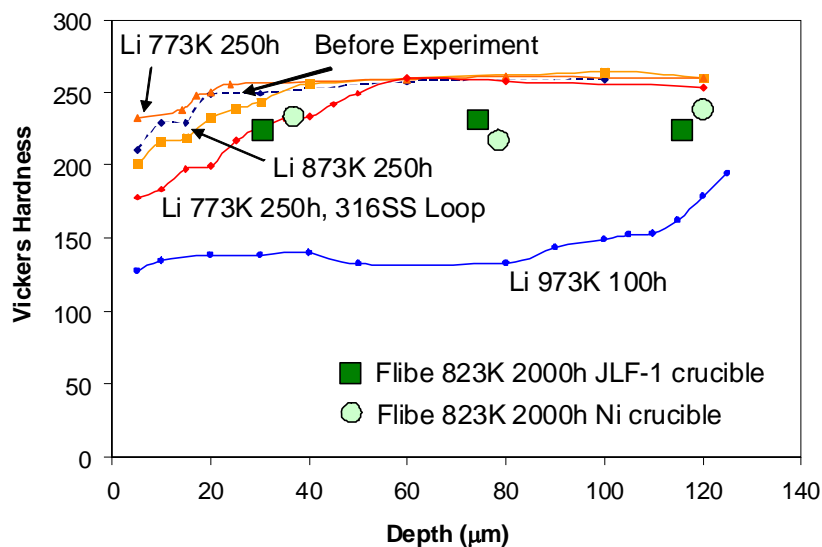


FIG. 6. Depth distribution of Vickers hardness.

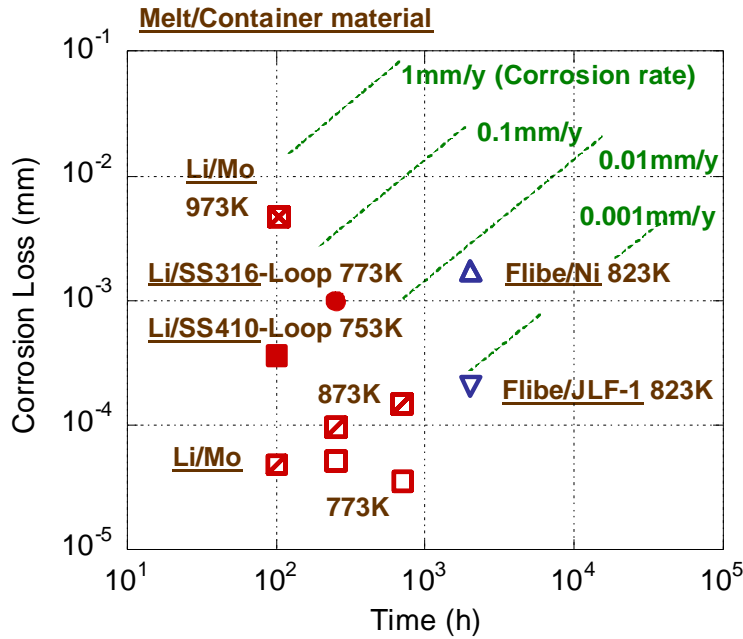
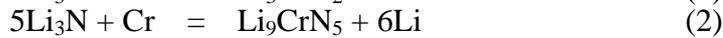
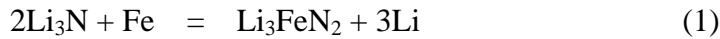


FIG. 7. Corrosion loss as a function of the exposure time in the present experiments.

significantly increase the solubility of many elements in Li, such as Fe and Cr by the chemical equations: [11]



Therefore, N is highly suspected to cause the weight loss. It was reported that the impact of N was limited when N level is lower than 100ppm [11] but the corrosion drastically increased with the increase of N concentration [10]. In the present experiment, level of N in Li was much higher at 973K than that at 873K. The possible chemical reactions by eqs. (1) and (2) may strongly promote the dissolution of alloy elements at 973K.

The weight loss per unit area of the specimen, Δm , equals the amount of dissolution of the alloy elements to Li and is expressed as:

$$\Delta m = VC_s/S \quad (3)$$

where V is the Li weight, (46g in the present static tests), C_s is the concentration of alloy element in Li and S is the specimen surface area contacting Li ($2.9 \times 10^{-4} \text{ m}^2$ in the present study).

In the present study N level in Li was 60wppm after exposure at 873K. Assuming that all the N reacts with Fe following the equation (1), 119wppm Fe will dissolve into Li. The concentration of Fe in Li will then be $C_{s1} = 60\text{g/m}^3$ (119wppm). On the other hand, the solubility of Fe and Cr in Li at 600°C is 16.0wppm (4appm) and 14.6wppm (4appm), respectively, at 873K [12]. If Fe and Cr dissolve in Li independently to the solubility limit, the total concentration is calculated to be $C_{s2} = 15\text{g/m}^3$ ($16.0 + 14.6 = 30.6$ wppm) assuming no reaction with N. The weight loss of the specimens can be predicted using eq. (3) and C_{s1} (N-Reaction Model) or C_{s2} (Solubility Model). The same procedure can be taken for the case of 973K, 100h using the solubility data and the measured N level (630 wppm).

Fig. 8 shows the relation of the measured and the predicted corrosion loss by exposure to Li. The fact that the prediction with the N-Reaction Model agrees with the measurements much better than that with the Solubility Model suggests that the dissolution of the alloy element

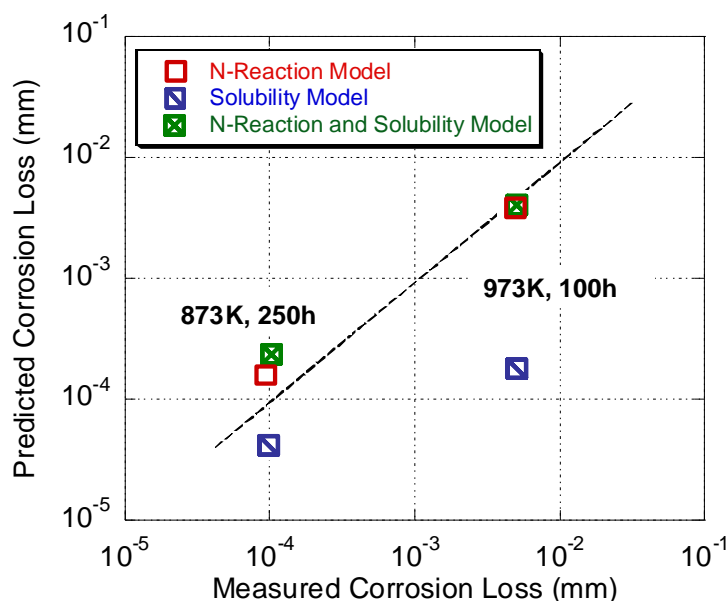


FIG. 8. Relation between the measured and the predicted corrosion loss of JLF-1 by exposure to Li

was induced predominantly by the reaction with N in Li. Therefore it was suggested that the corrosion loss rate of RAFM by liquid Li can be reduced by reducing the level of impurity N in Li.

The key corrosion process of Flibe is the competing process of fluoridation and oxidation. In Ni crucible, weight loss was enhanced by one order compared with that in JLF-1 crucible. In the test with Ni crucible, Fe precipitation occurred on the Ni crucible as shown in Fig. 5. Thus Fe transferred from JLF-1 plate to Ni crucible surface through Flibe.

Possible mechanism for the enhancement of the weight loss and the precipitation of Fe on the surface of Ni crucible is electrochemical reaction among JLF-1, Flibe and Ni crucible. Since JLF-1 plate was not completely insulated from Ni crucible, the plate and the crucible could form a circuit of electrochemical cell. Cell potential is determined by the difference between electrode potentials between JLF-1 plate and Ni crucible. At the beginning, cell potential can be as high as the difference between JLF-1 and Ni, and then it should decrease when Ni crucible is covered with Fe or Fe-Ni alloy formed on the surface. Fe transfer can last until the potential of the Ni-Fe alloy coverage decrease into the one of JLF-1 plate. It was suggested that the corrosion loss rate of RAFM by Flibe can be reduced by avoiding the use of dissimilar materials in Flibe.

Pure Fe and W are known to be highly compatible with liquid Li and Flibe, respectively. Thus the enrichment of Fe and W near the surface by exposure to Li and Flibe, respectively, shown in Fig. 4, implies that the compatibility of the specimens would increase with the exposure time. Thus the rate of the corrosion loss could slow with the exposure time for the both cases.

The corrosion rates of RAFM by flowing Li-Pb were predicted by a modeling [13] and a good agreement with loop experiments was reported [8]. The corrosion rates of RAFM in Li and Flibe estimated based on the present experimental data by assuming constant corrosion rates are indicated in Fig. 9 comparing with the prediction for Li-Pb. Except at 973 K, the present data by static tests show relatively low corrosion rate. However, the limited data with flowing Li show comparable corrosion rate with Li-Pb. Further comparison requires the knowledge about the effects of the flow rate on the corrosion for Li and Flibe. The high corrosion rate of Li at 973 K is known to be due to high N level in Li occurred in the experiment. With the improvement of N control the corrosion at 973K is expected to be reduced significantly.

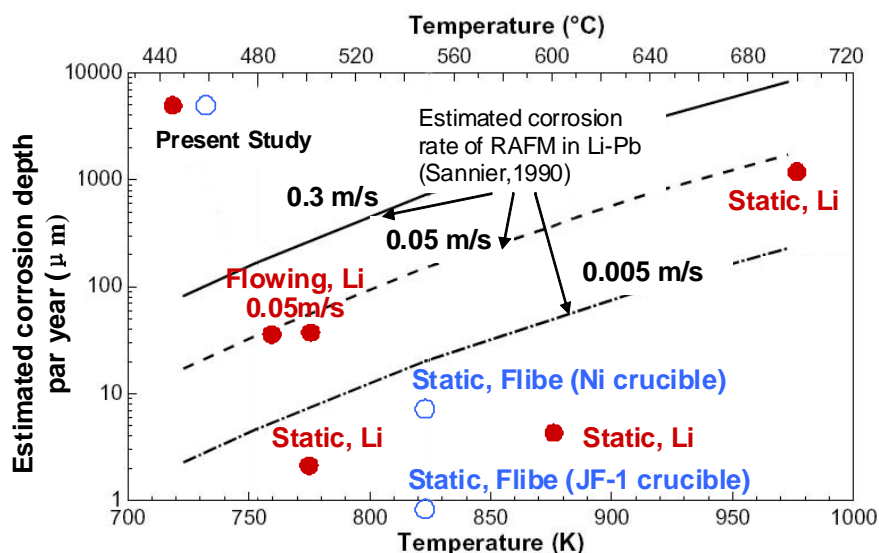


FIG. 9. Comparison of the present data with the calculation of RAFM corrosion rate by Li-Pb [13]

5. Conclusions

The exposure of RAFM to liquid Li induced depletion of carbon and resulting transformation of martensitic phase to ferritic phase. The phase change and the corrosion were enhanced in flowing Li. Model estimation showed that the dissolution of the alloy element was induced predominantly by the reaction with N in Li. The corrosion of RAFM with Flibe was induced by fluoridation and oxidation, and can be enhanced by the electrochemical circuit effects. The corrosion loss rate of RAFM by liquid Li and Flibe would be reduced by reducing the impurity N level in Li and by avoiding the use of dissimilar materials in Flibe, respectively.

Acknowledgements

This work was supported by NIFS Budget Code NIFS07KOBFO13, NIFS08UCFF002, NIFS08UCFF004, and Grant-in-Aid for Scientific Research (A), (2007-2009) 19206100.

References

- [1] B.G. Hong, D.W. Lee, S.J. Wang, Y. Kim, W. K. In, K.H. Yoon, *Fusion Eng. Des.*, 82 (2007) 2399-2405.
- [2] A. Sagara, O. Mitarai, S. Imagawa, et al., *Fusion Eng. Des.*, 81 (2006) 2703-2712.
- [3] Y. Poitevin, L.B. Boccaccini, A. Cardella, L. Giancarli, R. Meyder, E. Diegele, et al., *Fusion Eng. Des.* 75-79 (2005) 741-749.
- [4] e.g. P.F. Tortorelli, *J. Nucl. Mater.* 155-157 (1988) 722-727.
- [5] D. A. Petti., G.R. Smolik, M.F. Simpson, J. P. Sharpe, R.A. Anderl, S. Fukada, Y. Hatano, M. Hara, Y. Oya, T. Terai, D.-K. Sze, S. Tanaka, *Fusion Eng. Des.* 81 (2006) 1439-1449.
- [6] Q. Xu, T. Nagasaka and T. Muroga, *Fusion Science and Technol.* 52 (2007) 609-612.
- [7] T. Nagasaka, M. Kondo, H. Nishimura, T. Yakata, N. Noda., T. Muroga, A. Sagara, A. Suzuki and T. Terai, "Long Term Corrosion Test on JLF-1 Steel in Static High Purity Flibe", presented at 17th TOFE (2006) and submitted to *J. Nucl. Mater.*
- [8] J. Konys, W. Krauss, Z. Voss and O. Wedemeyer, *J. Nucl. Mater.* 367-370 (2007) 1144-1149.
- [9] M. Nagura, M. Kondoh, A. Suzuki, T. Muroga and T. Terai, *Fusion Science and Technol.* 52 (2007) 625-629.
- [10] O. K. Chopra and D.L. Smith, *J. Nucl. Mater.* 141-143 (1986) 566-570
- [11] R. J. Pulham and P. Hubberstey, *J. Nucl. Mater.* 115 (1983) 239-250.
- [12] M.W. Leabenworth, R.E. Cleary, *Acta Metall.* 9 (1961) 519-520
- [13] J. Sannier, T. Flament, A. Terlain, in: *Proceedings of the 16th SOFT 3-7 September, 1990*, London, UK, p. 901.